Zero discharge fluid dynamic gauging for studying the swelling of soft solid layers

Shiyao Wang and D. Ian Wilson*

Revised Manuscript

IE 2015 019564

Ind. Eng. Chem. Res. Des.

July 2015

Department of Chemical Engineering & Biotechnology
New Museums Site
Pembroke Street
Cambridge
CB2 3RA
UK

*Corresponding author

Dr Ian Wilson

Tel +44 1223 334791
FAX +44 1223 334796
E-mail diw11@cam.ac.uk

Zero discharge fluid dynamic gauging for studying the swelling of soft solid layers

Shiyao Wang and D. Ian Wilson

Department of Chemical Engineering and Biotechnology, New Museums Site, Pembroke Street, Cambridge, CB2 3RA, UK

Abstract

A bench-top device fluid dynamic gauging device to study the swelling or shrinking of soft solid layers immersed in a liquid environment *in situ* and in real time is demonstrated. A particular feature is that the volume of liquid is isolated, hence the name Zero net discharge Fluid Dynamic Gauging (ZFDG), which renders ZFDG suitable for aseptic operation. For the 1.78 mm nozzle diameter used here, calibration tests gave a resolution of ± 5 μm and uncertainty of ± 10 μm. Computational fluid dynamics simulations indicated that the shear stress imposed on a layer being gauged differed between the successive suction and ejection stages in ZFDG. The swelling of polyvinyl acetate (PVA) layers (about 1 mm dry thickness) and gelatin films (50-80 μm dry thickness) in aqueous solutions is reported as demonstration of a ZFDG application. There was good agreement with more cumbersome gravimetric methods. Gelatin swelled noticeably faster at high pH, above the pKa values of proline and hydroxyproline. Fitting the gelatin swelling data to a power law model indicated 'sub-Fickian' behaviour with a 'diffusion index' which increased with pH.

Keywords: cleaning, fluid dynamic gauging (FDG), PVA, gelatin, thickness, swelling

1. Introduction

In the chemical and biotechnological sectors, fouling is generally defined as the accumulation of unwanted material on solid surfaces with detrimental consequences, *i.e.* fouling layers are unwanted coatings. Fouling can result in high maintenance costs, low process efficiency and additional capital expenditure. It is therefore essential to understand the interactions between deposits and flowing fluids in order to prevent the former attaching, or to promote their detachment (cleaning). This requires both modelling and experiments in monitoring and quantifying the growth and removal of fouling deposits.

During cleaning, it is challenging to identify the extent of cleaning and the mechanism involved. Many fouling deposits are generated in liquid environments: as such, they are soft solids and are deformed, or weaker, once the layer is removed from its native liquid environment. Biofilms are examples: these often collapse when removed from water. Furthermore, properties of the layer may change over time. The technique of fluid dynamic gauging (FDG) was developed to measure the thickness and estimate the mechanical strength of soft solid layers immersed in liquid *in situ* and in real time.[1, 2] It does not require knowledge of physical and chemical properties of the layer except the presence of a locally stiff surface. It has advantages over other techniques, such as ultrasound and magnetic resonance imaging, in being relatively cheap and compatible with liquids at different temperatures and composition.

This paper reports a step change in FDG measurement, called zero net discharge fluid dynamic gauging (ZFDG) wherein the total liquid volume remains constant during measurement. In previous FDG measurements, liquid was continuously added or withdrawn, which is undesirable for aseptic operation or when costly or hazardous liquids are used. For example, Chew *et al.*[3] had to use full fume extraction when using FDG to study the cleaning of polymer reactor soiling layers by solvents including methylethylketone. The ZFDG concept was demonstrated in principle by Yang *et al.*[4]: this paper demonstrates its application in a semi-automated device that could, with further automation, be made to scan over a surface in a similar manner to the FDG device described by Gordon *et al.*[5]. The key difference in these measurements with ZFDG is that the liquid is retained in the system and its volume could be reduced to less than 1 L if needed. Moreover, measurements could be made at intermittent intervals, so that the layer is exposed to quiescent liquid between gauging operations.

Figure 1 illustrates the principles of ZFDG operation. The schematic shows the gauge nozzle geometry and dimensions. The nozzle is located near the surface, at clearance h, and liquid is ejected from or sucked into the nozzle at mass flow rate $\dot{m}$. The pressure drop across the nozzle, ΔP, is measured and is related to $\dot{m}$, nozzle lip width, w_r, nozzle rim thickness, w_e, nozzle throat diameter d_t, and clearance, h:

$$\Delta P = f\left(\dot{m}, \frac{h}{d_t}, \frac{w_r}{d_t}, \frac{w_e}{d_t}\right) \quad (1)$$

ΔP is expressed as the discharge coefficient, C_d, which is the ratio of actual and ideal mass flowrates, *i.e.*

$$C_d = \frac{\dot{m}_{actual}}{\dot{m}_{ideal}} = \frac{4\dot{m}}{\pi d_t^2 \sqrt{2\rho\Delta P}} \quad (2)$$

where ρ is the gauging liquid density. For a given geometry and flow rate, C_d is a function of h/d_t alone: measuring C_d allows the distance h to be calculated. By alternatively ejecting or sucking liquid at a fixed, low flow rate through the nozzle, measurements of ΔP can be made with no change in the total volume of liquid in the system over an extended period of time. This is the ZFDG concept: the individual components were demonstrated by Yang et al.[4], supported by computational fluid dynamics simulations of the flow patterns in ejection and suction.

Calibration is performed on a flat clean solid substrate, and ΔP is measured by adjusting the nozzle-substrate distance, h_0, at constant $\dot{m}$. Calibration plots present discharge coefficient, C_d, against dimensionless clearance, h_0/d_t. When a fouling layer is present, the nozzle-substrate distance, h_0, is known from independent measurements. ΔP is measured at different nozzle locations (z) and nozzle–soil clearance, h, is determined using the calibration plot. The deposit thickness is calculated from

$$\delta = h_0 - h \quad (3)$$

This paper demonstrates the operation of an automated ZFDG device. Calibration testing on uncoated substrates is used to establish the accuracy of the device. The results are compared with predictions from computational fluid dynamics (CFD) simulations, which allow the shear stress imposed on the surface to be calculated. Application of the ZFDG device to study the swelling behaviour of soft solids is demonstrated using polyvinyl acetate (PVA) and gelatin layers in aqueous solution. The results from the latter studies are compared with gravimetric swelling data and simple swelling models.

2. ZFDG Apparatus

2.1. Test rig set-up

Figure 2 shows photographs and a schematic of the apparatus. The syringe pump (Harvard Apparatus PHD Ultra™ Series pump; Hamilton® Glass syringe, i.d. 32.97 mm) controls the flow rate and direction. The accuracy in $\dot{m}$ is 1% of the set value, measured using separate tests. The gauging liquid is contained in a Perspex tank (280×280×160 mm^3: the liquid depth

is 120 mm). The nozzle is installed at the end of a long stainless steel tube (length L = 310 mm), sealed by two O-rings, and the nozzle – surface clearance is automatically controlled by a stepper motor (Zaber Technologies, T-LSR075B, CE). The zero position is set by using a feeler gauge with known thickness (*e.g.* 0.1 mm) and calibration tests are started from h_0 = 5.0 mm.

The substrate in these tests were usually 50 mm diameter 316 stainless steel discs, approximately 1.0 mm thick. In calibration tests the nozzle is moved towards the substrate until it reached h_0 = 0.1 mm, at which point the pressure drop across the nozzle usually exceeds the pressure transducer operating limit (7.0 kPa Honeywell® 24PCE analogue differential pressure transducer). At each nozzle location, ΔP is measured: that acquired while the syringe pump is running is denoted ΔP_{dyn}; the static measurement, ΔP_{static}, is recorded after the pump stops, in order to correct for any hydrostatic component in the pressure drop. Data collection and processing are performed using LabVIEW® (National Instruments™), which also controls the nozzle location and syringe pump motion. The apparatus is designed to move the nozzle and tank separately: the lateral position was adjusted manually in these tests.

Aqueous gauging solutions were prepared using deionised water (pH 5.6), adjusted to various pH values up to 11.6 by adding 1 M NaOH solution. Tests were performed at 16.5 °C and atmospheric pressure. Mass flow rates of 0.17 – 0.90 g/s were used, giving Reynolds numbers at the nozzle throat, defined as $Re_t = 4\dot{m}/\pi\mu d_t$, of 105 – 567, where μ is the viscosity of the gauging liquid.

2.2. Calibration protocol

The nozzle is moved towards the substrate, alternatively ejecting and sucking liquid at each nozzle location. ΔP is recorded at clearances from 5.0 mm to 0.5 mm at steps of 0.1 mm, and from 0.5 mm to 0.1 mm at steps of 0.02 mm, giving more increments in the useful measurement region ($0.05 < h/d_t < 0.20$). The control software waits for the ΔP reading to reach steady state. Calibration plots obtained with the nozzle moving away from the substrate gave identical results.

3. Materials and Methods

A PVA glue and gelatin were selected as test materials as they swell noticeably in aqueous solution but do not dissolve significantly in water at room temperature. PVA layers were prepared on Perspex® (polymethylmethacrylate) plates: gelatin layers employed the 316 stainless steel discs used in the calibration tests. The Perspex substrates were cleaned by washing in deionised water, soaking in ethanol and drying in air. 316 SS substrates were soaked in acetone then dried in air.

PVA (Evo-Stik™ glue: 56 wt% water, determined by drying to completion) layers were prepared by squeezing 1.2 g of glue on to a Perspex disc and allowing surface wetting to draw the drop into a uniform film. This was dried for 94 h at 16.5 °C, giving a 1.66 mm thick layer with liquid content 15.8 wt%. PVA samples were studied using deionised water as gauging liquid (pH = 5.6).

Gelatin coatings were prepared by a similar method, using a solution prepared by adding 9 g of powdered beef gelatin (84 wt% protein, 15 wt% water, 1 wt% carbohydrate; Dr. Oetker) to 100 ml deionised water followed by gentle heating (30 min at 125 °C) to dissolve the solids. 2 ml solution was pipetted on to the disc surface and surface tension spread the liquid out to give a thin, even layer. The sample was air dried (16.5°C, ~24 h, density ~ 1.23 g/ml) before being stored chilled. The procedure gave uniform, relatively dry (~ 10-20 wt% water content) colourless layers, with thicknesses measured by digital micrometer (Mitutoyo) ranging from 50 to 80 μm.

Gravimetric swelling tests were performed using a simple immersion arrangement. Coated plates were immersed in a large volume of solution. After given soaking times, plates were taken out of the solution and surface liquid removed using a paper towel. The wet mass, m_t, was measured using a precision balance and the thickness, δ, by a digital micrometer. The voidage of the layer, ε_g, was calculated from

$$\varepsilon_g = 1 - \frac{m_s}{m_t} \tag{4}$$

where m_s is the initial dry mass of solids in the layer. 2 – 3 repeats were performed for each pH. Equation (4) assumes that the initial voidage of the layer is negligible. The soaking time count was restarted when the plate was returned to the solution. Trials where plates were removed and weighed a different number of times showed little variation.

In ZFDG tests, the initial dry thickness of gelatin layer was measured using the digital micrometer. Immersing the sample in the solution and starting measurements took about 20 s. The syringe alternatively ejected then withdrew liquid at each nozzle location. Gauging was stopped for 20 s periods to reduce deformation by the liquid. The pressure drop across the nozzle was recorded continuously and when this approached the pre-set upper limit the clearance was adjusted, moving the nozzle away from the layer in the swelling tests reported here. The liquid volume fraction, ε_g, was calculated in a similar fashion to above, via

$$\varepsilon_z = 1 - \frac{\delta_s}{\delta_t} \tag{5}$$

where δ_s is the dry layer thickness at $t = 0$, and δ_t is the swollen layer thickness at time t.

4. Modelling

4.1 CFD Studies of ZFDG flows

The fluid dynamic gauging measurement technique relies on the pressure drop across the nozzle being dominated by losses in the region bounded by the layer and the gauging nozzle, and at the nozzle throat. The shear rates generated in this region can be high and can thus cause large shear stresses to be imposed on the surface being tested. It is therefore helpful to estimate these stresses in case deformation of the layer occurs.

The gauging liquid is Newtonian and the flows lie in the laminar or inertial regime. CFD simulations similar to those reported by Chew et al.[2] and Yang et al.[5] were performed for the geometry of the ZFDG apparatus using the COMSOL Multiphysics® finite element analysis software tool installed on a desktop PC (3.90 GHz Intel® Core™ i7-3770 CPU and 16 GB RAM). The surface being gauged is assumed to be flat and perpendicular to the nozzle axis. The geometry is complex so the domain is discretised using tetrahedral mesh elements. The solution approach is to set $\dot{m}$ and the clearance, h_0: ΔP is extracted from the converged solution and C_d calculated. Ejection and suction modes employ similar boundary conditions but the mesh has to be optimised for each case owing to differences between the respective flow patterns.

4.1.1 Governing equations

The flow is isothermal and incompressible: in ZFDG testing measurements are made once initial transients have subsided so steady state flow patterns are calculated in the CFD

simulations. The gauging liquid is Newtonian with constant viscosity. The Navier-Stokes (N-S) and continuity equations are

$$\rho\left(\frac{\partial \boldsymbol{v}}{\partial t} + \boldsymbol{v}\cdot\nabla\boldsymbol{v}\right) = -\nabla P + \mu\nabla^2\boldsymbol{v} + \rho\boldsymbol{g} \quad (6)$$

$$\nabla\cdot\boldsymbol{v} = 0 \quad (7)$$

where $\boldsymbol{v}$ is the velocity vector. The gravitational term is neglected[2] and a pressure difference is imposed to drive the flow. The N–S equations then simplify to

$$\boldsymbol{v}\cdot\nabla\boldsymbol{v} = -\frac{-\nabla P}{\rho} + \frac{\mu\nabla^2\boldsymbol{v}}{\rho} \quad (8)$$

The fluid properties are summarised along with the dimensions in Table 1.

4.1.2 Boundary conditions and meshing

The boundaries to the CFD simulation domain are shown schematically in Figure 3 and the boundary conditions are listed in Table 2. The flow at the top end of the tube – the inlet in ejection mode and the outlet in suction mode – is assumed to be fully developed Poiseuille flow with flow rate set by the experimental values of $\dot{m}$. Fluid leaves or enters the domain (in ejection or suction mode, respectively) via Boundary E: this reflects the experimental case more accurately and also gives good simulation convergence. For both modes, boundary A is the axis of symmetry and there is no radial flow across this axis. Boundaries marked 'C' and 'D' are modelled as impermeable walls and there is no slip on these.

The bulk liquid is effectively stagnant and the nozzle is axisymmetric. The system is modelled as a quadrant in 3-D and the final solution mesh used in the simulations is shown in Figure 4. The computer memory limited the number of mesh elements to approximately 3×10^6. The highest pressure and velocity gradients occur under the nozzle rim and along the lip, and the mesh element density was greatest in these regions. Tetrahedral mesh elements were specified using the software's mesh generation package. The mesh patterns for ejection and suction were quite similar, except that there is a recirculation zone in the expanding part of nozzle in suction mode. More mesh elements were specified in these regions as a result. The computing time for each simulation varied from several minutes to a couple of hours.

4.1.3 CFD validation

The simulation results were checked by comparing predicted and measured pressure drops, as well as mass conservation. The inlet and outlet mass flow rates were compared for all values studied (0.17 – 0.90 g/s, in ejection and suction mode) and gave good agreement. Increasing the number of mesh elements did not affect the mass balance noticeably, but did give rise to differences in the pressure drop and thus the calculated C_d values. Mesh elements were added progressively in the regions of high shear rate. Table 3 shows that C_d approaches an asymptote as the number of mesh elements was increased, at the cost of computational effort. The predicted values of C_d differ between ejection and suction mode, which is related to the presence of the recirculation zones and larger regions of higher velocity in the latter mode. Similar results were reported by Yang *et al.*[4] in their simulations which employed cylindrical, 2-D geometries. The agreement between the simulated and experimental values in Table 3 is good, while the difference in magnitude between the simulated C_d values in suction and ejection matches the difference in the experimental values.

The solutions reported here were obtained by running a series of simulations with progressively lower viscosity, using the converged solution from one to start the next test. The CPU time for ejection mode calculations is larger than for suction mode when fewer mesh elements are used because the embedded solver in COMSOL takes longer to resolve the jet in the region underneath the nozzle for a low viscosity liquid. By comparison, the difference is relatively small when the largest number of mesh elements was used.

4.1.4 Surface shear stress

The CFD simulations allow the shear stress imposed by the ZFDG flow on the surface being studied to be estimated. This can then be related to the stresses required to cause cohesive failure[4], and the adhesion between the layer and the surface[6]. Chew *et al.*[7] showed that the shear stress directly under the nozzle rim, τ_w, can be estimated from the results for laminar radial flow between two parallel discs, *viz.*

$$\tau_w = \frac{3\mu\dot{m}}{\pi\rho h^2 x} \tag{9}$$

where x is the distance from the nozzle centreline. The largest value of τ_w occurs at the inner rim of the nozzle, *i.e.* $x = 0.89$ mm for the nozzle employed in these tests. This analytical result

is compared with the shear stress distributions obtained from the simulations in the Supplementary Material.

4.2 Swelling Dynamics

Three quantitative models are used in this work to characterise the PVA and gelatin layer swelling kinetics.

I Power law mass uptake

Ritger and Peppas[8] reviewed polymer swelling behaviour and reported that swelling kinetics are often described by a simple power law relationship, *viz.*

$$m = m_\infty k_I t^n \tag{10}$$

where m is the solvent taken up after time t, m_∞ is the amount taken up at swelling equilibrium, t is the time immersed, k_I is a kinetic constant and n is the 'diffusion index'. Assuming that the solvent (water) uptake is uniformly distributed over the surface and the surface area and gelatin density do not change during the swelling process, the increase in mass is proportional to the change in thickness of the layer. This gives

$$\delta - \delta_0 = (\delta_\infty - \delta_0) k_I t^n \tag{11}$$

where δ_0 is the initial dry thickness, δ_∞ is the final thickness and δ is the layer thickness at time t. Regression fitting of swelling profiles (plots of δ against t) is used to identify the parameters $k_I (\delta_\infty - \delta_0)$ and n: the latter indicates the type of swelling mechanism, *e.g.* $n = 0.5$ being interpreted as Case I or 'Fickian' behaviour and $n = 1$ as Case II or chain relaxation.

II Second order swelling

Schott[9] proposed this model to fit the swelling dynamics observed with gelatin and cellulose in aqueous media. The rate of swelling is assumed to be proportional to

(i) The swelling capacity (fractional amount of swell), given by $(m_\infty - m)/m_\infty$, at time t, and

(ii) The internal specific boundary area, S_{int}, representing the sites in polymer networks that have not yet interacted with water at time t but will hydrate and swell in due course, given by

$$S_{int} = k' \left(\frac{m_\infty - m}{m_\infty} \right) \tag{12}$$

where k' is a geometrical factor accounting for interchain hydrogen bonds. Polymeric networks are held together by hydrogen bonds and other attractive forces between adjacent chains. When

solvent penetrates into the structure, these bonds are broken and new linkages are formed, particularly if the solvent promotes charge formation on the polymer. If there is charge formation, the polymer network expands to accommodate the influx of solvent caused by osmotic pressure. S_{int} is a significant parameter in this swelling model. The overall rate of solvent uptake (swelling) is then given by

$$\frac{dm}{dt} = k\left(\frac{m_\infty - m}{m_\infty}\right) S_{int} = kk'\left(\frac{m_\infty - m}{m_\infty}\right)^2 = k_{II}(m_\infty - m)^2 \tag{13}$$

where $k_{II} = \frac{kk'}{m_\infty{}^2}$.

Integrating from the initial condition, $m = m_0$ at $t = 0$, yields

$$m(t) = \frac{m_0 + m_\infty k_{II} t(m_\infty - m_0)}{1 + k_{II} t(m_\infty - m_0)} \tag{14}$$

Assuming uniform density and thickness across the layer gives

$$\delta = \frac{\delta_0 + \delta_\infty k_{II} t(\delta_\infty - \delta_0)}{1 + k_{II} t(\delta_\infty - \delta_0)} \tag{15}$$

III Swelling front model

In this case the polymer is assumed to swell instantaneously in the presence of an undefined level of solute, giving rise to a swelling front dividing a swollen region wherein the solute is present and a region into which the solute will move (see Figure 5). The rate of ingress of the swelling front is assumed to be controlled by Fickian diffusion or another process which follows similar dynamics. The thickness of the gel layer at time t can written as the sum of the thicknesses of the swollen and unswollen layers (δ_s and δ_u, respectively):

$$\delta(t) = \delta_s + \delta_u \tag{16}$$

The overall rate of layer growth is given by

$$\frac{d\delta}{dt} = \frac{d\delta_u}{dt} + \frac{d\delta_s}{dt} \tag{17}$$

Defining a swelling ratio, α, as

$$\alpha = -\frac{d\delta_s}{d\delta_u} \tag{18}$$

Equation (17) becomes,

$$\frac{d\delta}{dt} = \left(1 - \frac{1}{\alpha}\right)\frac{d\delta_s}{dt} \tag{19}$$

If the progress of the swelling front is controlled by Fickian diffusion for a dilute species, one can write

$$\frac{d\delta_s}{dt} = -\alpha\frac{d\delta_u}{dt} = \frac{k_{III}}{\delta_s} \tag{20}$$

where k_{III} is related to the diffusivity of the species. Integrating from $t = 0$, $\delta_s = 0$ gives

$$\delta_s = \sqrt{2k_{III}t} \tag{21}$$

Rearrangement gives

$$\Delta\delta = \delta - \delta_0 = \left(1 - \frac{1}{\alpha}\right)\sqrt{2k_{III}t} \tag{22}$$

The layer thickness is expected to increase with $t^{0.5}$, and to stop swelling when $\delta = \alpha\delta_0$.

5. Results and Discussion

5.1 ZFDG Calibration and Accuracy

Calibration tests were performed at room temperature with deionised water as the gauging liquid. The sets of calibration plots (C_d vs h_0/d_t) obtained using a flowrate of 0.33 g/s in Figure 6 show similar behaviour to that reported previously.[2, 5] For a fixed flow rate, ΔP is greatest and C_d smallest when the nozzle is close to the surface. C_d increases with increasing h/d_t and approaches an asymptote at large h/d_t; in this case $C_d \sim 0.40$. The value of the asymptote depends on Re_t. In this pressure mode gauging configuration, lower C_d values are preferred as the ΔP measured for a given flow rate is larger. The error bar associated with the uncertainty in the pressure transducer measurement becomes more significant at larger h/d_t. At small h/d_t values the shear stress imposed by the gauging liquid on the surface is large and there is thus a trade-off between measurement accuracy and measurement reliability.[10]

The range of h_0/d_t values in the inset in Figure 6 represent the optimal range of gauging conditions: the calibration plot is usefully close to linear in this region. The inset shows that there is good agreement between the experimental C_d values and those predicted by the CFD simulations in ejection mode. The measured suction mode values are noticeably smaller than the simulation values, which is attributed to limitations in the pressure transducer used. The trend is, nevertheless, reproducible and allows thickness measurements to be made with confidence.

The main uncertainties in measurements arise from the accuracy in determining the nozzle–substrate clearance, h_0, since ΔP is very sensitive to lower values of h. The accuracy of the mass flow measurements is good (less than 1% error). The pressure transducer uncertainty is reduced by amplification and filtering to increase the signal to noise ratio.

The accuracy was checked by comparing ZFDG measurements of the thickness of layers of waterproof tape which could be measured independently with a digital micrometer (Mitutoyo®). A typical tape thickness was 900 µm. ZFDG measurements were performed on the test layer at three flow rates (0.17 – 0.50 g/s) and the agreement with the micrometer value compared at each h/d_t. These tests indicated that the best agreement was obtained with h/d_t near 0.10, with an uncertainty of ± 10 µm. For a given flow rate, this corresponds to a given ΔP value: in practice, the nozzle is moved towards the surface until the pressure transducer reads this value, and the layer thickness can then be determined from Equation (3).

Dynamic thickness measurements on gelatin were performed using a flowrate of 0.33 g/s, changing h/d_t from 0.20 to 0.05 initially by increments of 0.01. Suction mode gave an accuracy of ±10 µm whereas ejection mode was less accurate, at ± 20 µm. The best resolution achieved was ~± 5 µm for measurements at $0.09 < h/d_t < 0.11$. When the syringe movement is initiated there is a brief disturbance in ΔP which lasted less than 1 s. These transients were eliminated from the data before processing.

5.2 Swelling of PVA layers

PVA layers were immersed in deionised water for about 5 hours. ZFDG measurements were taken continuously, with ejection and suction stages each lasting about 2 s. Figure 7(*a*) shows that swelling was still occurring at the conclusion of the test, at which point the liquid content had reached 28 wt% (*cf.* initial value of 15.8 wt%). The thickness measurements obtained from gravimetric testing are plotted alongside the ZFDG measurements and show very good agreement compared with the suction mode values: the ejection mode data also agree within the measurement uncertainty. The micrometer measurements are expected to underestimate the thickness at longer times due to the elasticity of the layer when compressed by the micrometer stub. Use of ZFDG to measure soft solids swelling *in situ*, making substantially more thickness measurements, is thereby demonstrated. Moreover, ZFDG avoids the challenges faced when

dealing with non-ambient temperatures, hazardous solvents or the requirements of aseptic operation.

There is a noticeable disagreement between ejection and suction measurements, although the difference lies within the measurement uncertainty. The difference between suction and ejection appears to be reset periodically, which corresponds to the time when the nozzle was moved upwards. This difference is attributed to deformation of the layer by the shear stresses imposed by the flow: the CFD simulations indicated that the largest τ_w values ranged from 2 to 20 Pa in these tests. The PVA material is viscoelastic: the consistency of the trends in successive suction and ejection measurements suggest that the interaction is primarily elastic and characterised by a short timescale. Interactions between the ZFDG liquid flow pattern and the layer is the subject of ongoing work.

Swelling in the PVA layer is expected to be driven by diffusion and chain relaxation. The absence of an equilibrium swelling state means that the data cannot be fitted to Model II. The ZFDG data are replotted in Figure 7(*b*) as $\Delta\delta$ vs t for comparison with Model I and show a reasonable fit to the suction data. The diffusion index, n, is close to 0.7 and indicates that this is an example of anomalous transport, combining Fickian diffusion with polymer relaxation due to internal stresses arising from swelling of the polymer. [11] For the anomalous transport, relaxation rate is a function of the balance of rigidity/flexibility, the degree of cross-linking, the length of side chains and pH.[12] The value of 0.7 indicates that polymer stretching, to accommodate the influx of liquid, is not instantaneous.

5.3 Swelling of gelatin

The swelling of gelatin layers with an initial dry thickness of 50 - 80 μm was studied at various pH conditions at room temperature. The current ZFDG configuration does not allow the nozzle to scan the surface[13] and thereby collect several data sets from each sample, so several samples (at least four) were tested at each condition in order to gauge the variability between samples. Figure 8 shows acceptably good intra-sample reproducibility for notionally identical experiments at pH 9.4. Ejection mode profiles showed the same behaviour, whereas there were noticeable differences between the two modes for the PVA layers in Figure 7. Standard deviations of 40 μm and 34 μm were obtained using ejection and suction modes, respectively.

The initial loading of the sample and initiating the flow took about 30 s, during which there is a fast hydration step driven by diffusive, chemical and electrostatic interactions.[14] The layer is then approximately 100 μm thick. Thereafter the rate of swelling decreases: Gordon *et al.*[15] observed similar behaviour using a scanning FDG system, and reported that the swollen layer thickness approached an asymptote after 4 hours, i.e. at longer times than the 5000 s duration of these tests.

The impact of the stress imposed by the gauging flow was investigated by using different flow rates ($\dot{m}$ = 0.33 – 0.67 g/s) in notionally identical tests. Figure 9 shows the evolution of gelatin layer thickness at pH 6.8 (tap water), determined in suction mode. There is a consistent, small difference in measured thickness, with the largest value recorded for the highest flow rate and thus suction stress which would cause the layer to swell. This confirms that the gel has an elastic response to stress. Further work could include systematically switching between suction and ejection to determine the mechanical properties of the interface. This result indicates that it is important to use consistent suction or ejection conditions when comparing factors, particularly when collecting data for quantitative modelling.

ZFDG measurements showed generally good agreement with gravimetric testing: this is discussed in detail below.

Effect of pH

Alkaline solutions are generally cheap cleaning agents that can break down protein layers through the action of hydroxyl ions.[16] The swelling of gelatin in alkali at lower pH is governed by osmotic pressure differences arising between the protein phase and the external solution.[17] As a protein, however, the biopolymer contains ionisable functional groups. When there is electrostatic repulsion among the groups, it leads to chain expansion which can affect the macromolecular chain relaxation.[18] The swelling mechanism then becomes more relaxation-controlled. Ionisation is expected to have an influence when the pH in the layer approaches the pK_a values for the amine groups in gelatin: for glycine (21 wt% of total), at 9.6; for glutamic acid (10 wt%), at 9.7; for proline (12 wt%), at 10.6; and for hydroxyproline (12 wt%), also at 10.6.[19]

Figure 10 shows swelling profiles recorded for pH ranging from 5.6 to 11.6. In all cases the rapid initial hydration phase is completed within 200 s and is followed by slower swelling. There is a noticeable effect of the strongest alkali after 8 min (~ 500 s), with a swelling rate about twice that of the other cases. After 5000 s the extent of swelling at pH 11.6 was about 50% greater than that at pH 11. By comparison, the extent of swelling at pH 11 after 5000 s (~ 0.8 mm in Figure 10) was about 50% greater than that at pH 5.6 (~ 0.55). Gordon et al.[15] reported similar differences between pH 11.6 and 9.4 (achieved in their studies using 0.03 M buffer solutions). The large increase in swelling at pH 11.6 is attributed to deprotonation of the amine groups on proline and hydroxyproline driving charge repulsion within the layer. It is noticeable that the amount of extra repulsion was relatively weak at pH 11. This could be due to depletion of the H^+ concentration as the solvent diffuses into the layer and is consumed in protonation steps: a high concentration is needed to drive the reaction to completion.[20]

Comparison with gravimetric tests

Figure 11 presents the results obtained from ZFDG and gravimetric testing on notionally identical gelatin layers immersed in deionised and tap water (pH 5.6 and 6.8, respectively, differing due to the presence of dissolved CO_2), and alkaline solutions with pH 8.5 - 11.6. The data are presented as the thickness, δ (measured directly by micrometer or ZFDG) and volume fraction of solution ε. The latter was calculated assuming that the density of water and polymer are approximately equal: for gravimetric testing, ε_g is given by equation (4) and for ZFDG studies, ε_Z is given by equation (5). The initial gravimetric voidage is calculated from

$$\varepsilon = 1 - \frac{\frac{m_{dry}}{\rho_{dry} * (\frac{\pi d^2}{4})}}{\delta_{dry}} \tag{23}$$

where d is the disc diameter. The thickness measurements show very good agreement between the two techniques, within experimental uncertainty, until higher pH conditions. At pH 11.6 there is an extensive swelling and the difference in δ values is significant. This consistent difference is attributed to the compression imposed by the micrometer stub measurement action: the more highly swollen layer is expected to be weaker and thus less able to resist the stub compression. At this pH the δ values collected in suction and ejection modes at longer times differed by about 10%, indicating some elasticity in the highly swollen layer.

Both techniques show that ε increases rapidly initially, from about 20% to 80% within 8 min, followed by slow swelling to an asymptotic value of around 90%. The initial rate of solution uptake is greater at higher pH and the asymptote is approached more quickly. There is a difference between ε_g and ε_Z values at higher pH, which is thought to arise from mass loss when handling and drying the highly swollen layer as well as dissolution of the gelatin. The layers all followed the same relationship between (overall) voidage and layer thickness, shown in Figure 12, indicating that pH was determining the rate at which the material swelled.

Modelling swelling

Plotted alongside the ZFDG thickness data in Figure 11 are the lines of best fit obtained for the power law model, Equation (10) to the gravimetric data. Similarly good agreement, albeit yielding different model parameters, was obtained by fitting Equation (11) to the ZFDG data sets. The parameters obtained by fitting suction mode ZFDG data are summarised in Table 4. The diffusion index, n, increases with increasing pH and approaches 0.5, the value associated with Fickian transport, at higher pH. This transition between 'sub Fickian' behaviour, which is dependent on the relative contribution of penetrant diffusion and polymer relaxation, and Fickian with increasing pH, is attributed to differences between the solvent penetration rate and the polymer chain relaxation rate.[21]. The swelling ratio, calculated at the end of the test is also reported in Table 4 and increases by a factor of 3.6 across the pH range.

Figure 13 shows an example of the fit of the three swelling models to the experimental data obtained for gelatine layers contacted with pH 11.6 solution. The models were fitted to data after the hydration stage: Models I and II give reasonable agreement with the suction and ejection mode data over the time period studied ($R^2 > 0.99$), whereas Model III did not give good agreement initially ($t < 360$s). There is a systematic difference between suction and ejection thickness measurements at this pH, which is attributed to elasticity in the layer.

Fitting the power law model, Equation (11) to the data (Figure 13(*a*)) gave a diffusion index of $n = 0.49$ (see Table 4). The second order model (Equation 15, (Figure 13(*b*)) shows good agreement except in the early stage of ($t < 200$ s), where it over-predicts the layer thickness: this is likely due to hydration. The equilibrium thickness of the gelatine layer, δ_∞, can be estimated from the model parameters, from

$$\delta_{\infty,est} = \frac{\delta_\infty * (\delta_\infty - \delta_0) * k_{II}}{(\delta_\infty - \delta_0) * k_{II}} \quad (24)$$

giving δ_∞ = 2.36 ±0.02 mm and 2.27 ±0.02 mm for the ejection and suction case, respectively. This final thickness, of approximately 2.3 mm, is four times the initial wet thicknesses of the layers (prepared at pH 6.8), indicating that the polymer wants to adopt a more open configuration at the higher pH – which is consistent with repulsion between charged chains.

At pH 11.6 the power law index is 0.49 and the swelling front model, (Figure 14(*c*), Equation (22)) is then of similar form and gave a reasonable fit. k_{III} gives an order of magnitude estimate of a Fickian diffusion coefficient as 3.8×10^{-10} m^2/s. This is comparable with the average diffusivity of hydroxyl ion in a whey protein gel at pH 12.2 solution of 1.15×10^{-9} mm^2/s reported by Mercadé-Prieto & Chen.[22]

The effect of pH on the power law model parameters is summarised in Figure 14. The 'diffusion index' *n* differed from 0.5 at pH values other than 11.6 so the fit of the swelling front model was poorer (data not reported). There is a systematic effect of pH on ε_∞ and δ_∞, in accordance with charge-induced swelling at pH values above 9.4.

ZFDG demonstrates significant advantages over gravimetric testing: (*i*) the samples do not have to be removed from solution; (*ii*) more frequent measurements can be made (and with scanning, more sites tested), (*iii*) softer layers can be studied reliably; and (*iv*) measurements are not influenced by the user's experimental technique. Furthermore, ZFDG tests can be conducted at other temperatures (and pressures) readily, rendering it a powerful tool for studying fouling or cleaning.

6. Conclusions

The concept of automated zero discharge fluid dynamic gauge has been demonstrated. The ability to operate with a fixed volume of liquid has advantages when using hazardous liquids or reagents with limited availability. The experimental calibration curves showed similar behaviour between suction and ejection stages. This difference was evident in CFD simulations and there was reasonable agreement between experimental and simulation C_d values.

Calibration testing identified a useful measurement range, $0.05 < h_0/d_t < 0.20$, with a maximum resolution of ± 5 μm, and accuracy of ± 10 μm for the thickness measurements. CFD simulations indicated that the shear stress imposed on the surface being gauged varied more noticeably in ejection mode, so suction mode should be favoured for measuring thicknesses of deformable layers at a given flow rate.

The swelling characteristics of layers prepared from PVA glue in water and thinner gelatin layers at different pH were studied. ZFDG measurements gave good agreement with simple (and more time-consuming) gravimetric methods. The PVA layers exhibited swelling of the 'anomalous transport' type. Gelatin behaviour depended on pH, with the diffusion index of a simple power law model increasing with pH. These results are consistent with previous studies.

Acknowledgements

Development of the ZFDG concept was supported by the Royal Society's Paul Instrument Fund. Funding from Fitzwilliam College for Shiyao Wang is also gratefully acknowledged.

Reference

(1) Tuladhar, T.R.; Paterson, W.R.; Macleod, N.: Wilson, D.I., Development of a novel non-contact proximity gauge for thickness measurement of soft deposits and its application in fouling studies. *Can. J. Chem. Eng.* **2000**, **78**, 935-947.

(2) Chew, J.Y.M.; Cardoso, S.S.S.; Paterson, W.R.; Wilson, D. I. CFD studies of dynamic gauging. *Chem. Eng. Sci.* **2004**, **59**(16), 3381–3398.

(3) Chew, J.Y.M.; Tonneijk, S.J.; Paterson, W.R.; Wilson, D.I. Mechanisms in the solvent cleaning of emulsion polymerization reactor surfaces. *Ind. Eng. Chem. Res.* **2005**, **44**(13),4605-4616.

(4) Yang, Q.; Ali, A.; Shi, L.; Wilson, D.I. Zero discharge fluid dynamic gauging for studying the thickness of soft solid layers. *J. Food Eng.* **2014**, **127**, 24–33.

(5) Gordon, P.W.; Brooker, A.D.M.; Chew, J.Y.M.; Wilson, D.I.; York, D.W. A scanning fluid dynamic gauging technique for probing surface layers. *Measurement Sci. and Tech.* **2010**, **21**(8), 85103.

(6) Saikhwan, P.; Chew, J.Y.M.; Paterson, W.R.; Wilson, D.I. Swelling and its suppression in the cleaning of polymer fouling layers. *Ind. Eng. Chem. Res.* **2007**, **46**(14), 4846-4855.

(7) Chew, J.Y.M.; Höfling, V.; Augustin, W.; Paterson, W.R.; Wilson, D.I. A method for measuring the strength of scale deposits on heat transfer surfaces. *Dev. Chem. Eng. Mineral Proc.* **2005**, **13**(1/2), 21-30.

(8) Ritger, P.L.; Peppas, N.A. A simple equation for description of solute release II. Fickian and anomalous release from swellable devices. *J. Controlled Release* **1987**, **5**, 37–42.

(9) Schott, H. Swelling kinetics of polymers. *J. Macromolecular Sci., Part B:Physics* **1992**, **31**:1, 1-9.

(10) Salley, B.; Gordon, P.W.; McCormick, A.J.; Fisher, A.C.; Wilson, D.I. Characterising the structure of photosynthetic biofilms using fluid dynamic gauging. *Biofouling* **2012**, **28**:2, 159–173.

(11) Thomas, N.L.; Windle, A.H. A deformation model for case II diffusion. *Polymer* **1980**, **21**, 613–619.

(12) Ganji, F.; Vasheghani-Farahani, S.; Vasheghani-Farahani, E. Theoretical description of hydrogel swelling: A review. *Iranian Polymer J.* **2010**, **19**(5), pp.375–398.

(13) Gordon, P.W.; Schöler, M.; Föste, H.; Helbig, M.; Augustin, W.; Chew, Y.M.J.; Scholl, S.; Majschak, J-P.; Wilson, D.I. A comparison of local phosphorescence detection and fluid dynamic gauging methods for studying the removal of cohesive fouling layers: effect of layer roughness, *Food Bioprod. Proc.* **2014**, **92**, 46–53.

(14) Ofner III, C. M.; Schott, H. Swelling studies of gelatin I: Gelatin without additives. *J. Pharma. Sci.* **1986**, **75**, 790–796.

(15) Gordon P.W.; Brooker A.D.M.; Chew Y.M.J.; Letzelter, N.; York D.W.; Wilson D.I. Elucidating enzyme-based cleaning of protein soils (gelatine and egg yolk) using a scanning fluid dynamic gauge, *Chem. Eng. Res. Des.* **2012**, **90**, 162-171.

(16) Lelieveld, H. L. M. *Hygiene in Food Processing*, **2003**,Woodhead Publishing Series in Food Science, Technology and Nutrition

(17) Bowes, J.H.; Kenten, R.H. The swelling of collagen in alkaline solutions. 1. Swelling in solutions of sodium hydroxide. *Biochem. J.*, **1950**, **46**(1), 1–8.

(18) Gierszewska-Drużyńska, M.; Ostrowska-Czubenko, J., Mechanism of water diffusion into noncrosslinked and ionically crosslinked chitosan membranes. **2011**, *XVII Seminar and Workshop "New Aspects of the Chemistry and Applications of Chitin and its Derivatives", Warsaw*.

(19) Stevens, P.V. Gelatine. *Food Australia* **1992**, **44**(7), 320-324.

(20) Mercadé-Prieto, R; Paterson, W. R.; Chen, X.D.; Wilson, D. I. Diffusion of NaOH into a protein gel. *Chem. Eng. Sci.* **2008**, **63**(10), 2763–2772.

(21) Dengre, R.; Bajpai, M.; Bajpai, S.K. Release of Vitamin B12 from poly (N-vinyl-2-pyrrolidone)-crosslinked polyacrylamine hydrogels: a kinetic study, *J. Appl. Polym.Sci.* **2000**, **76**, 1706-1714.

(22) Mercadé-Prieto, R.; Chen, X.D. Dissolution of whey protein concentrate gels in alkali. *AIChE J.*, **2006**, **52**(2), 792–803.

Nomenclature

Roman		
C_d	Fluid discharge coefficient	-
d	Disc diameter	m
d_i	Inner diameter	m
d_t	Diameter of nozzle throat	m
d_o	Outer diameter	m
h	Nozzle-layer clearance	m
h_0	Nozzle-substrate clearance	m
H	Height of liquid immersed in tank	m
k	Rate constant	-
k_{I}	Rate constant for power law model	-
k_{II}	Rate constant for second order	-
k_{III}	Rate constant for swelling front model	-
m	Mass	kg
m_s	Initial dry mass of model layers	kg
m_t	Mass in time t	kg
m_∞	Mass in the equilibrium state	kg
$\dot{m}$	Mass flow rate of gauging liquid	kg/s
n	Diffusion index	-
ΔP	Differential pressure ($\Delta P_{\mathrm{dyn}} - \Delta P_{\mathrm{static}}$)	Pa
r	Radial co-ordinate	m
R^2	Coefficient of determination	-
Re_t	Reynolds number at nozzle throat	-
S_{int}	Internal specific boundary area	m^2
t	Time	s
v_m	Mean velocity	m/s
W	Width	m
w_e	Nozzle rim thickness	m
w_r	Nozzle rim width	m
x	Horizontal coordinate	m
z	Vertical coordinate	m

Greek

α	Swelling ratio	-
δ	Layer thickness	m
δ_s	Swollen layer thickness	m
δ_t	Swollen layer thickness at time t	m
δ_u	Unswollen layer thickness	m
δ_0	Initial dry layer thickness	m
δ_∞	Final layer thickness	m
$\delta_{\infty,\,est}$	Estimated final layer thickness	m
ε	Water/solvent volume fraction	-
ε_g	Water/solvent volume fraction in gravimetric measurement	-
ε_s	Initial water/solvent volume fraction	-
ε_Z	Water/solvent volume fraction in ZFDG	-
ε_∞	Final water/solvent volume fraction	-
θ	Nozzle converging angle	°
ρ	Density of gauging liquid	kg/m^3
τ_w	Wall shear stress	Pa
μ	Liquid viscosity	Pa s

Acronyms

CFD	Computational fluid dynamics
PT	Pressure transducer
PVA	Poly vinyl acetate
RMSE	Root mean-square deviation
ZFDG	Zero (net) discharging fluid dynamic gauging

List of Table Captions:

Table 1. CFD simulation dimensions and fluid parameters

Table 2. Boundary conditions in CFD simulations (see Figure 3 for labelled locations)

Table 3. Effect of mesh density on discharge coefficient calculated from CFD simulations. Test case conditions: $\dot{m}$ = 0.33 g/s, h_0/d_t = 0.05, deionised water, 16.5 °C.

Table 4. Power law (Model I) parameters obtained from least square regression of ZFDG thickness data in Figure 11.

Table 1. CFD simulation dimensions and fluid parameters

Parameters	Value
d_t	1.78 mm
d_i	4 mm
d_o	8 mm
H	120 mm (liquid depth)
W	280 mm
L	310 mm
μ	1.12 mPa s
ρ	997.3 kg/m^3
temperature	16.5 °C

Table 2. Boundary conditions in CFD simulations (see Figure 3 for labelled locations)

Boundary	Description	Boundary condition
A	Axis of symmetry	No radial flow, *i.e.* v_x=0
B	Gauging nozzle tube	Fully developed laminar flow at end, v_x=0 $\dot{m}$ is defined by syringe pump, with $v_x = \frac{4\dot{m}}{\rho\pi d_i^2}(1 - \frac{4x^2}{d_i^2})$ (ejection) $v_x = \frac{-4\dot{m}}{\rho\pi d_i^2}(1 - \frac{4x^2}{d_i^2})$ (suction)
C, D	Wall: no slip and impermeable	$v_x = 0$; $v_z = 0$
E	Open boundary	Parallel streamlines, $p = 0$

Table 3. Effect of mesh density on discharge coefficient calculated from CFD simulations. Test case conditions: $\dot{m}$ = 0.33 g/s, h_0/d_t = 0.05, deionised water, 16.5 °C.

Number of mesh elements	Ejection mode		Suction mode	
	C_d	CPU time/s	C_d	CPU time/s
Experimental value	0.092±0.017	-	0.085±0.013	-
67144	0.097	181	0.092	134
117567	0.095	388	0.089	200
292937	0.094	966	0.086	442
868145	0.093	1552	0.086	5246
3131868	0.093	6660	0.086	6961

Table 4. Power law (Model I) parameters obtained from least square regression of ZFDG thickness data in Figure 11.

pH	$(\delta_\infty-\delta_0)*k_I$ /mm s^{-n}	n -	RMSE* -	R^2	$SR=\frac{\delta_\infty}{\delta_0}$
5.6	0.055	0.28	0.031	0.997	7.1
6.8	0.023	0.38	0.069	0.995	6.2
8.5	0.020	0.42	0.027	0.999	8.1
9.4	0.036	0.35	0.050	1.000	10.7
10.5	0.020	0.43	0.044	0.998	12.5
11.0	0.017	0.46	0.013	1.000	12.8
11.6	0.023	0.49	0.067	0.999	25.4

* RMSE – root mean square error

List of Figure captions

Figure 1. Schematic elevation of ZFDG geometry. Nozzle dimensions: $\theta = 54°$, $d_t = 1.78$ mm, $d_i = 4$ mm, $w_e = 0.2$ mm, $w_r = 1.32$ mm. Dotted streamline – ejection mode; dashed streamline – suction mode (showing flow recirculation).

Figure 2. (*a*) Schematic view of ZFDG test rig; photographs of (*b*) ZFDG test rig with (*c*) 1.78 mm i.d. nozzle throat. Labels: A - syringe pump; B - stepper motor; C - pressure transducer (PT); D – nozzle.

Figure 3. Boundaries in CFD simulations. Label descriptions given in Table 2. O is the origin of the Cartesian coordinate frame.

Figure 4. Tetrahedral mesh of CFD simulation with 292937 elements. Inset shows detail of mesh elements around the nozzle throat.

Figure 5. Schematic of swelling front model at (a) $t = 0$, initial layer thickness, δ_0 and (*b*) time t, after liquid diffuses into the soft layer, giving swollen layer thickness, δ_s, unswollen layer thickness, δ_u and total layer thickness, $\delta(t)$.

Figure 6. Calibration plots, of C_d against dimensionless clearance h_0/d_t, for $\dot{m} = 0.33$ g/s water at 16.5°C. Symbols: square – ejection (E), triangle – suction (S). Inset compares experimental values with CFD predictions. Solid and dashed lines show simulation results for ejection and suction, respectively.

Figure 7. (*a*) Swelling of PVA glue film immersed in deionised water (pH = 5.6, 16.5 °C) with $\dot{m} = 0.50$ g/s. Gravimetric results are shown in black hollow circles. Representative error bars plotted. Symbols: square – ejection (E), triangle – suction (S). Inset compares experimental values with CFD predictions. Solid and dashed lines show simulation results for ejection and suction, respectively. δ_{final} is the maximum thickness measured. (*b*) Fit of power law model (Equation 11) to where $\Delta\delta = \delta(t) - \delta_0$, dotted line – ejection, and dashed line – suction.

Figure 8. Reproducibility testing. Suction mode data (decimated for clarity: 1 out of 40 data points is plotted) for four notionally identical tests for initially dry gelatine layers immersed in pH 9.4 solution (16.5 °C) at t = 0 s. $\dot{m}$ = 0.33 g/s (Re_t = 189). Sample initial wet thickness 1.02 ±0.01 mm: dry thickness: S1 - 63 ±10 µm, square symbols; S2 - 55 ±10 µm, diamonds; S3 - 52 ±10 µm, triangles; S4 - 51 ±10 µm, crosses. Error bars show maximum experimental uncertainty.

Figure 9. Swelling profiles of gelatine layers with initial thickness ~ 80 ±10 µm obtained with different gauging flowrates. pH 6.8 (tap water), suction mode.

Figure 10. Effect of pH on swelling profiles for gelatine layers. Data sets decimated for clarity (1 point per 40 is plotted). Conditions: 16.5 °C, suction mode, $\dot{m}$ = 0.33 g/s. The inset shows the evolution of the swelling ratio ($SR = \frac{\delta_t}{\delta_0}$) calculated for pH = 11.6.

Figure 11. Swelling profiles (volume fraction, ε, against time – primary axis and thickness, δ, against time – secondary axis) for initially dry gelatine layers immersed in (a) deionised water (16.5 °C, pH 5.6), (b) tap water (16.5 °C, pH 6.8) and, (c) pH = 9.4, (d) pH= 10.5, (e) pH = 11, and (f) pH = 11.6 solution. Solid symbols – gravimetric data, hollow – ZFDG data ($\dot{m}$ = 0.33 g/s using suction mode). Square – ε, triangle – δ. Dashed and dotted lines show fitted power law models for thickness, δ, using gravimetric and ZFDG measurements respectively.

Figure 12. Evolution of liquid volume fraction against layer thickness for (*a*) ZFDG and (*b*) gravimetric measurements. Legend in (*a*) indicates pH.

Figure 13. Comparison of swelling models with ZFDG experimental data for gelatine layers at pH 11.6, 16.5 °C. (*a*) power law, equation (9); (*b*) Model II, equation (13); (c) swelling front, equation (20). Data decimated for clarity. Symbols: ejection – circle, solid line; suction – triangle, dashed line. Initial dry thickness 58 ±10 µm, $\dot{m}$= 0.33 g/s.

Figure 14. (*a*) Diffusional indices, *n*, from power law fitting, equation (9), at different pH for both ZFDG and gravimetric measurements. Symbols: hollow – ZFDG, solid –

gravimetric; circle – ε, and square – δ; $n = 0.5$ indicates Fickian diffusion. (*b*) Estimated final volume fraction of solvent, ε_∞ and thickness, δ_∞.

Supplementary Figure:

Figure S1. Shear stress imposed on the surface being gauged, from CFD calculations. Conditions: $\dot{m} = 0.33$ g/s (deionised water, 16.5 °C). Hollow symbols. Left– ejection, solid symbols, right – suction. Lines show analytical solution (denoted 'A') assuming radial flow between nozzle rim and substrate (Equation (9)). The position of the inner and outer edges of nozzle rim are indicated by black vertical dashed lines at $x = \pm 0.89$ mm and $x = \pm 2.21$ mm, respectively.

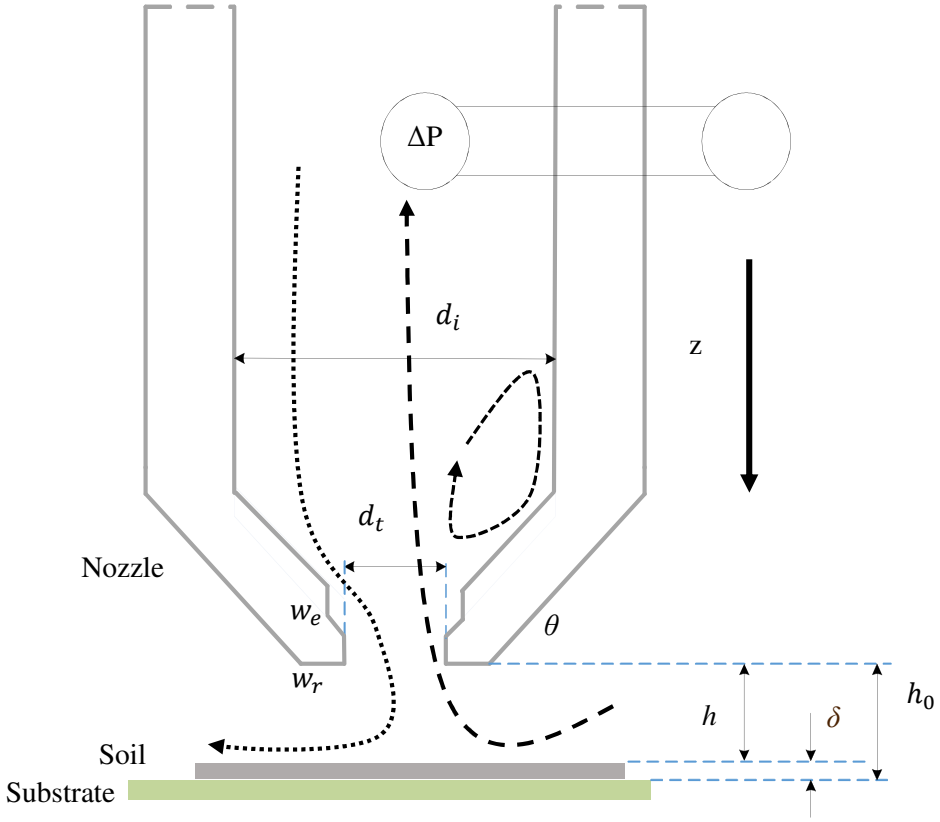

Figure 1. Schematic elevation of ZFDG geometry. Nozzle dimensions: $\theta = 54°$, $d_t = 1.78$ mm, $d_i = 4$ mm, $w_e = 0.2$ mm, $w_r = 1.32$ mm. Dotted streamline – ejection mode; dashed streamline – suction mode (showing flow recirculation).

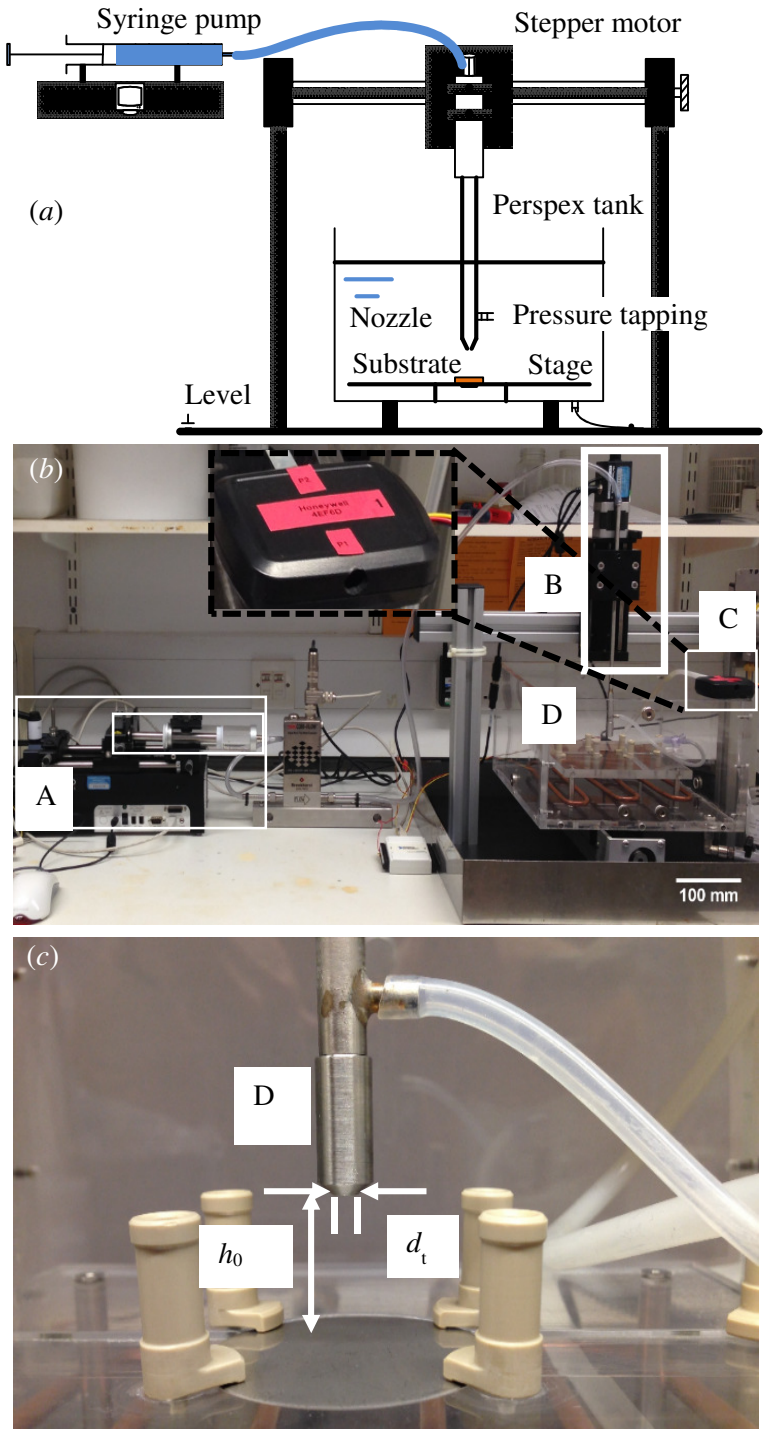

Figure 2. (*a*) Schematic view of ZFDG test rig; photographs of (*b*) ZFDG test rig with (*c*) 1.78 mm i.d. nozzle throat. Labels: A - syringe pump; B - stepper motor; C - pressure transducer (PT); D – nozzle.

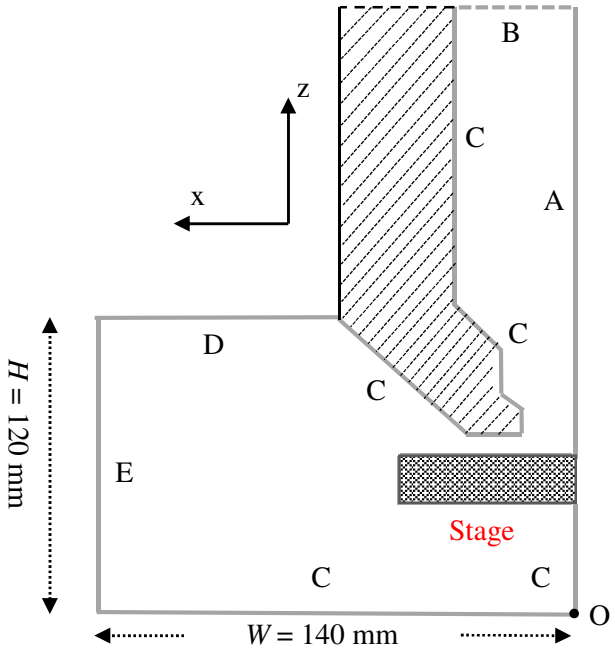

Figure 3. Boundaries in the FD simulations. Label descriptions are given in Table 2. O is the origin of the Cartesian coordinate frame.

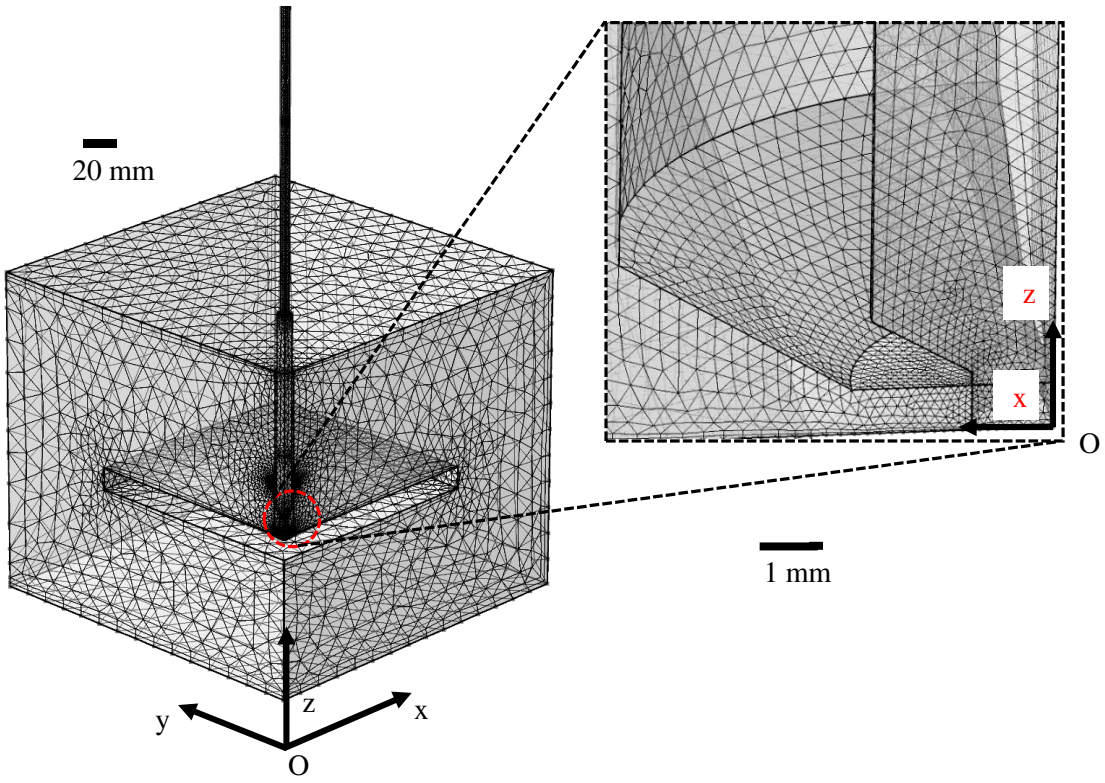

Figure 4. Tetrahedral mesh of CFD simulation with 292937 elements. Inset shows detail of mesh elements around the nozzle throat.

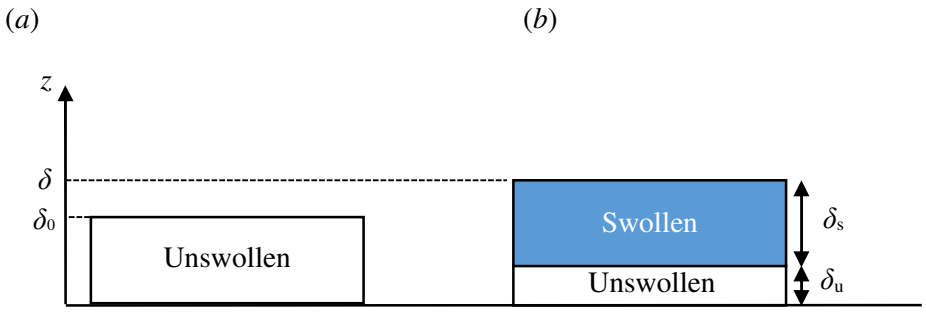

Figure 5. Schematic of swelling front model at (a) $t = 0$, initial layer thickness, δ_0 and (b) time t, after liquid diffuses into the soft layer, giving swollen layer thickness, δ_s, unswollen layer thickness, δ_u and total layer thickness, $\delta(t)$.

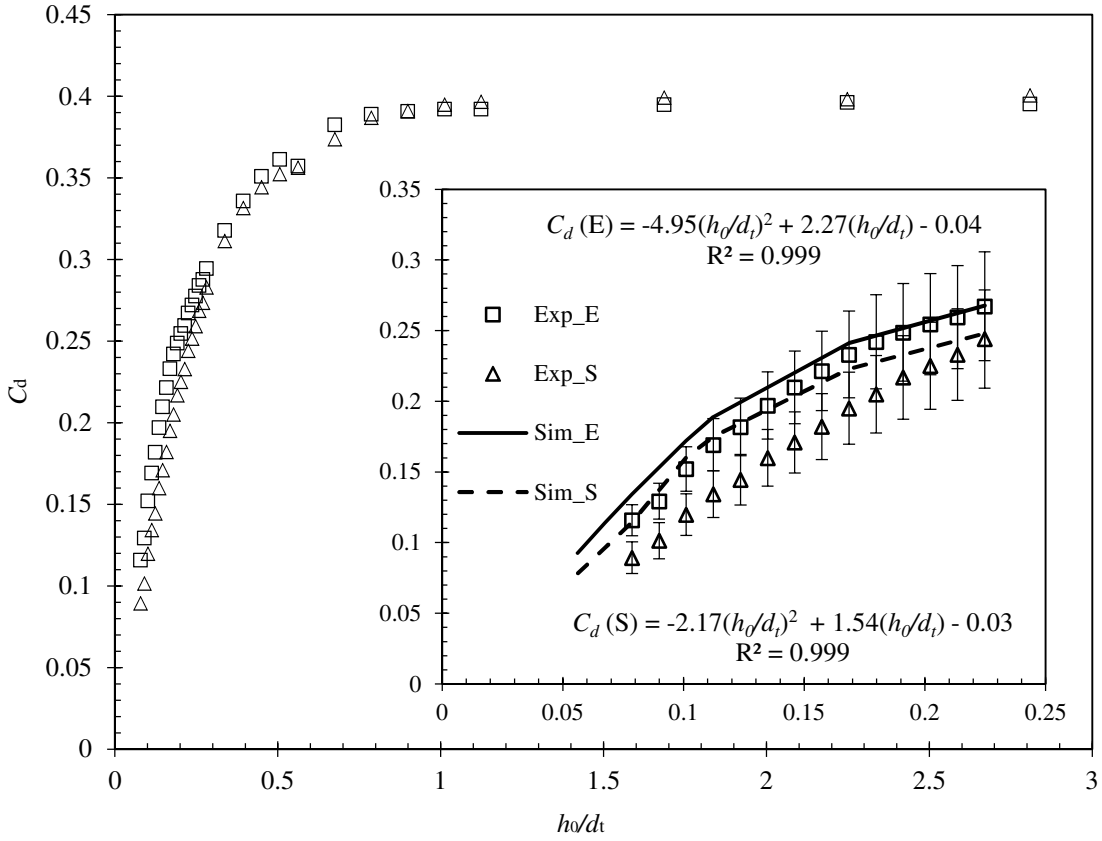

Figure 6. Calibration plots, of C_d against dimensionless clearance h_0/d_t, for $\dot{m}$ = 0.33 g/s water at 16.5°C. Symbols: square – ejection (E), triangle – suction (S). Inset compares experimental values with CFD predictions. Solid and dashed lines show simulation results for ejection and suction, respectively.

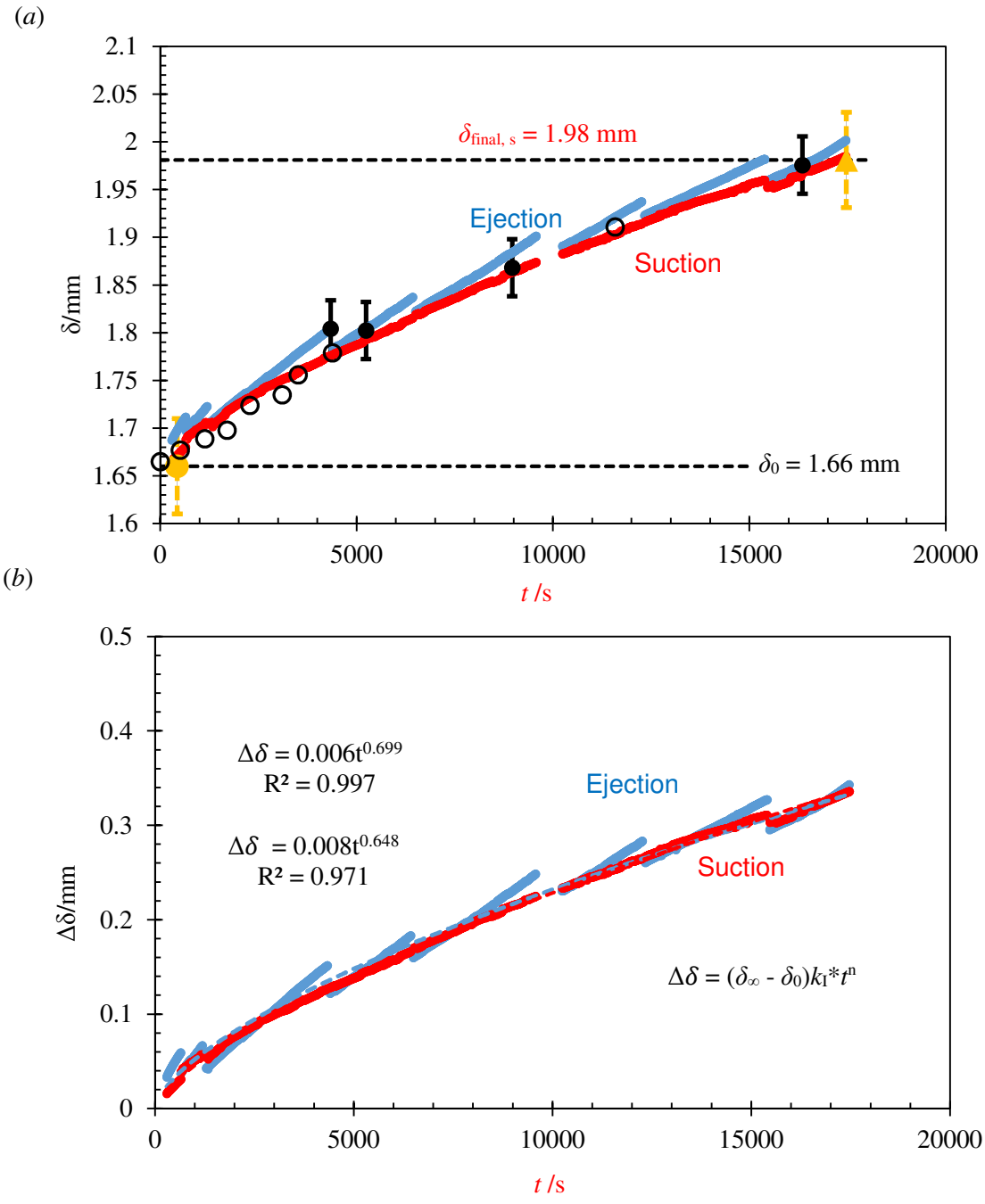

Figure 7. (*a*) Swelling of PVA glue film immersed in deionised water (pH = 5.6, 16.5 °C) with $\dot{m}$ = 0.50 g/s. Gravimetric results are shown in black hollow circles. Representative error bars plotted. Symbols: square – ejection (E), triangle – suction (S). Inset compares experimental values with CFD predictions. Solid and dashed lines show simulation results for ejection and suction, respectively. δ_{final} is the maximum thickness measured. (*b*) Fit of power law model (Equation 11) to where $\Delta\delta = \delta(t) - \delta_0$, dotted line – ejection, and dashed line – suction.

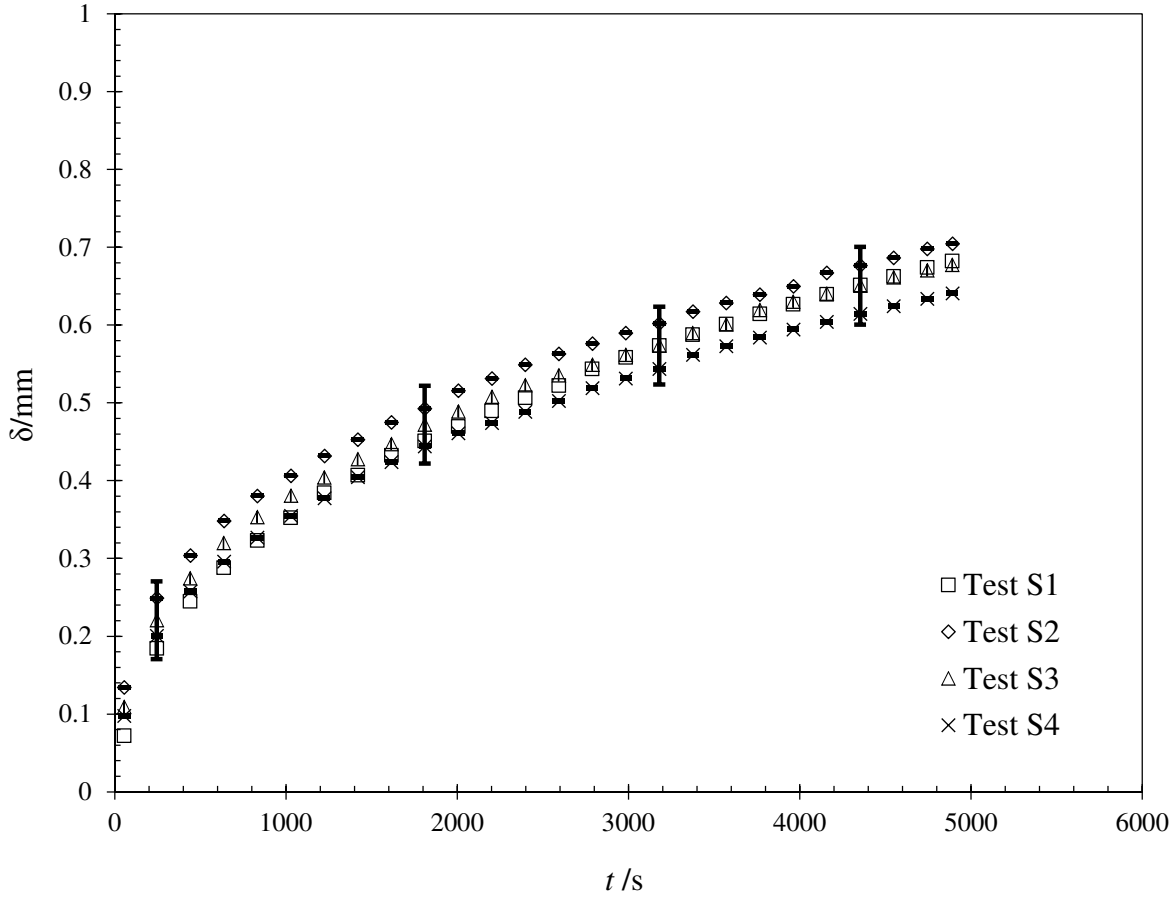

Figure 8. Reproducibility testing. Suction mode data (decimated for clarity: 1 out of 40 data points is plotted) for four notionally identical tests for initially dry gelatine layers immersed in pH 9.4 solution (16.5 °C) at $t = 0$ s. $\dot{m} = 0.33$ g/s ($Re_t = 189$). Sample initial wet thickness 1.02 ±0.01 mm: dry thickness: S1 - 63 ±10 μm, square symbols; S2 - 55 ±10 μm, diamonds; S3 - 52 ±10 μm, triangles; S4 - 51 ±10 μm, crosses. Error bars show maximum experimental uncertainty.

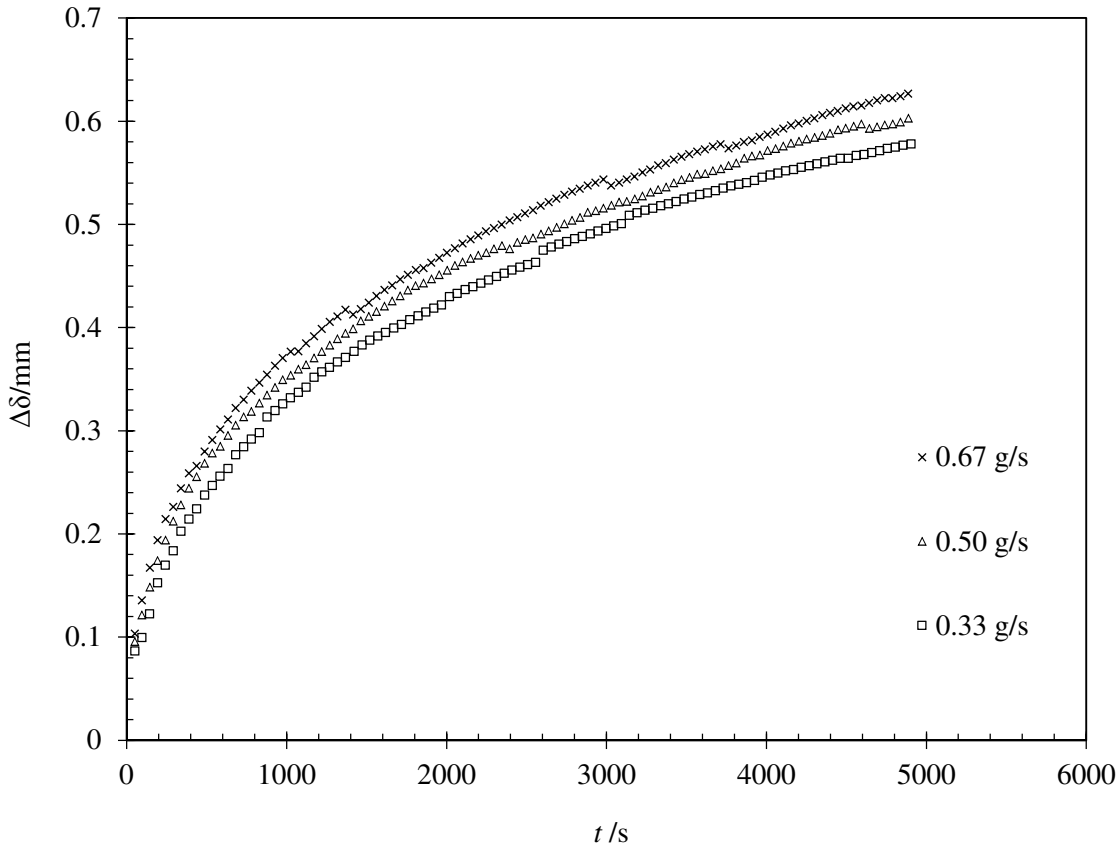

Figure 9. Swelling profiles of gelatine layers with initial thickness ~ 80 ±10 μm obtained with different gauging flowrates. pH 6.8 (tap water), suction mode.

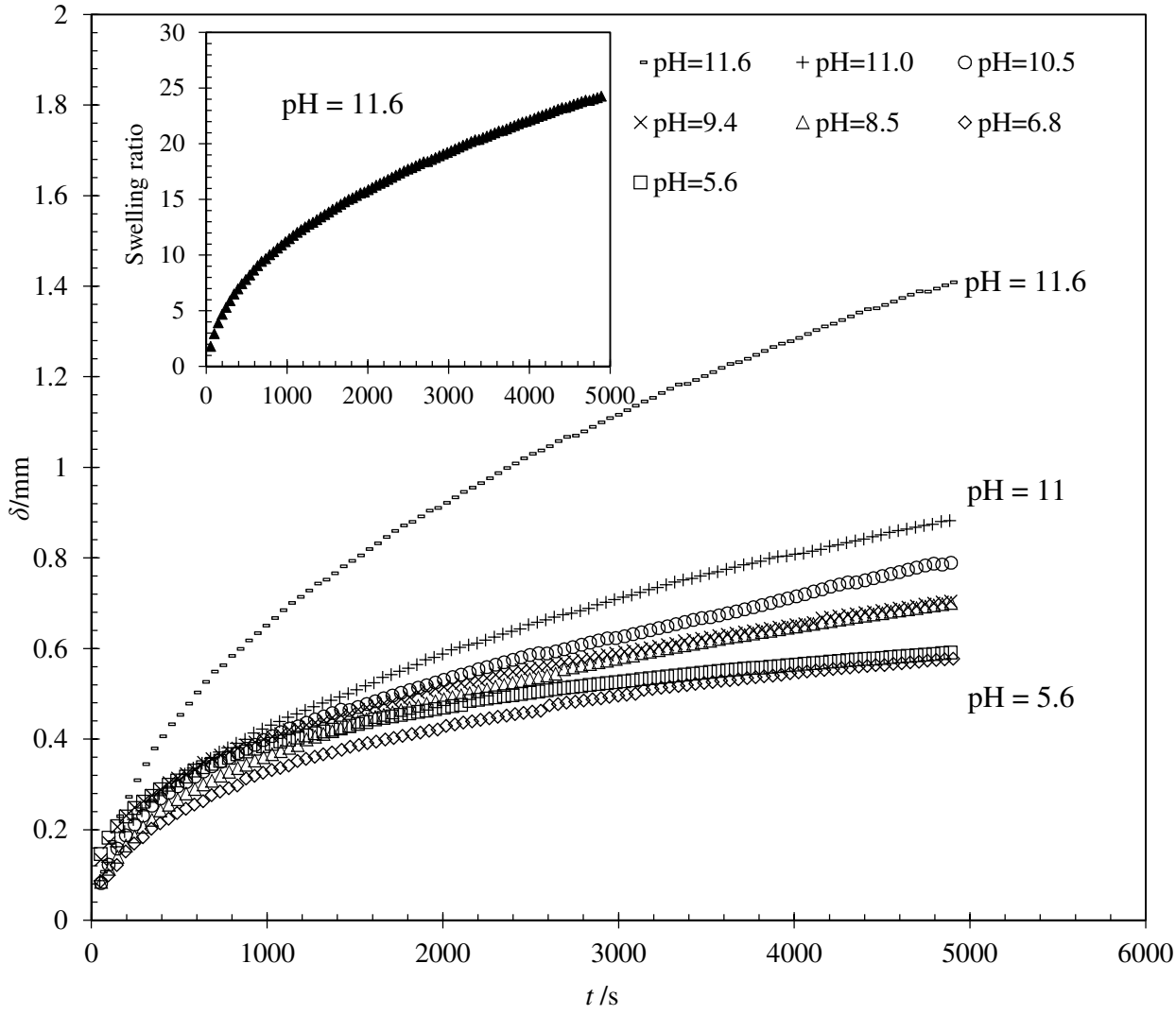

Figure 10. Effect of pH on swelling profiles for gelatine layers. Data sets decimated for clarity (1 point per 40 is plotted). Conditions: 16.5 °C, suction mode, $\dot{m}$ = 0.33 g/s. The inset shows the evolution of the swelling ratio ($SR = \frac{\delta_t}{\delta_0}$) calculated for pH = 11.6.

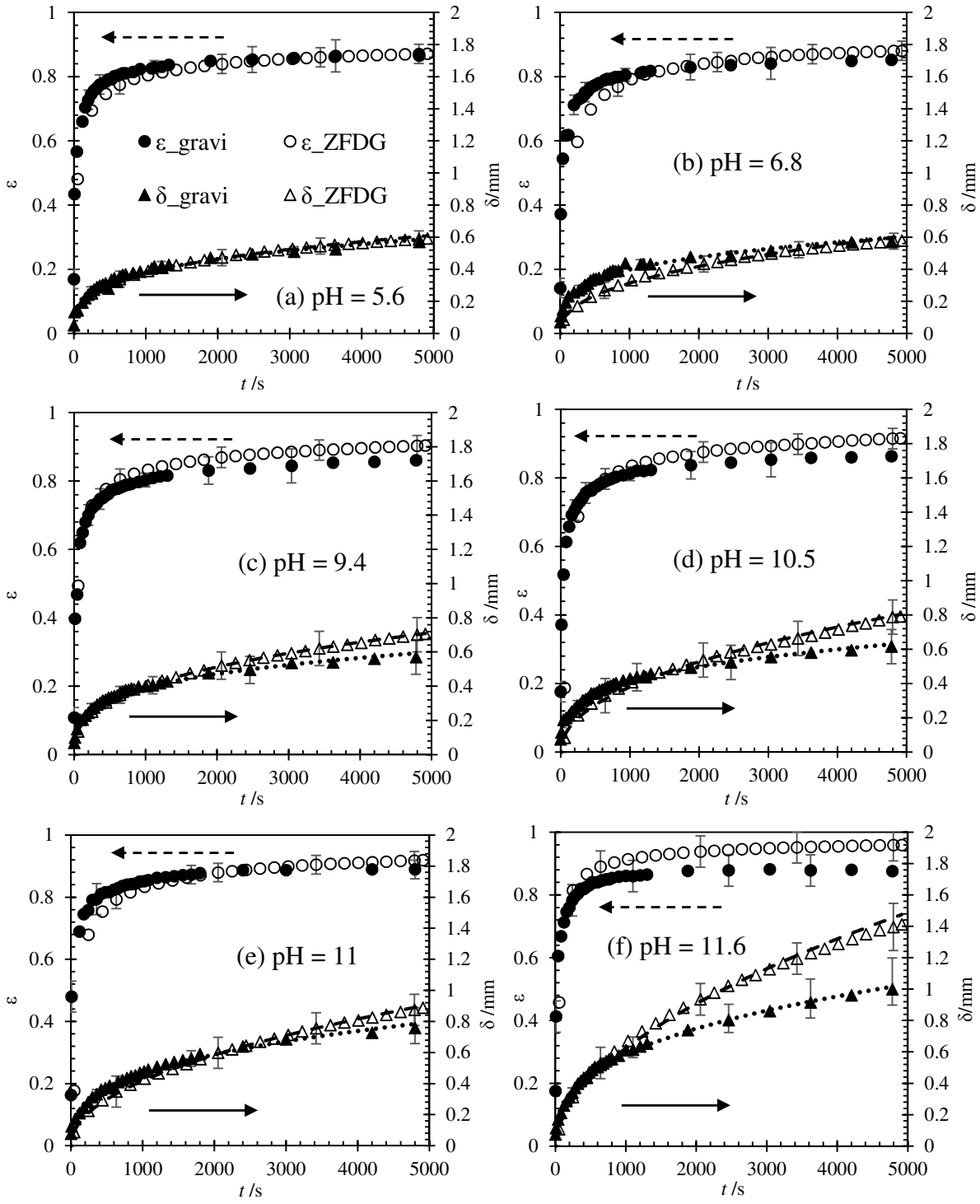

Figure 11. Swelling profiles (volume fraction, ε, against time – primary axis and thickness, δ, against time – secondary axis) for initially dry gelatine layers immersed in *(a)* deionised water (16.5 °C, pH 5.6), *(b)* tap water (16.5 °C, pH 6.8) and, *(c)* pH = 9.4, *(d)* pH= 10.5, *(e)* pH = 11, and *(f)* pH = 11.6 solution. Solid symbols – gravimetric data, hollow – ZFDG data ($\dot{m}$ = 0.33 g/s using suction mode). Square – ε, triangle – δ. Dashed and dotted lines show fitted power law models for thickness, δ, using gravimetric and ZFDG measurements, respectively.

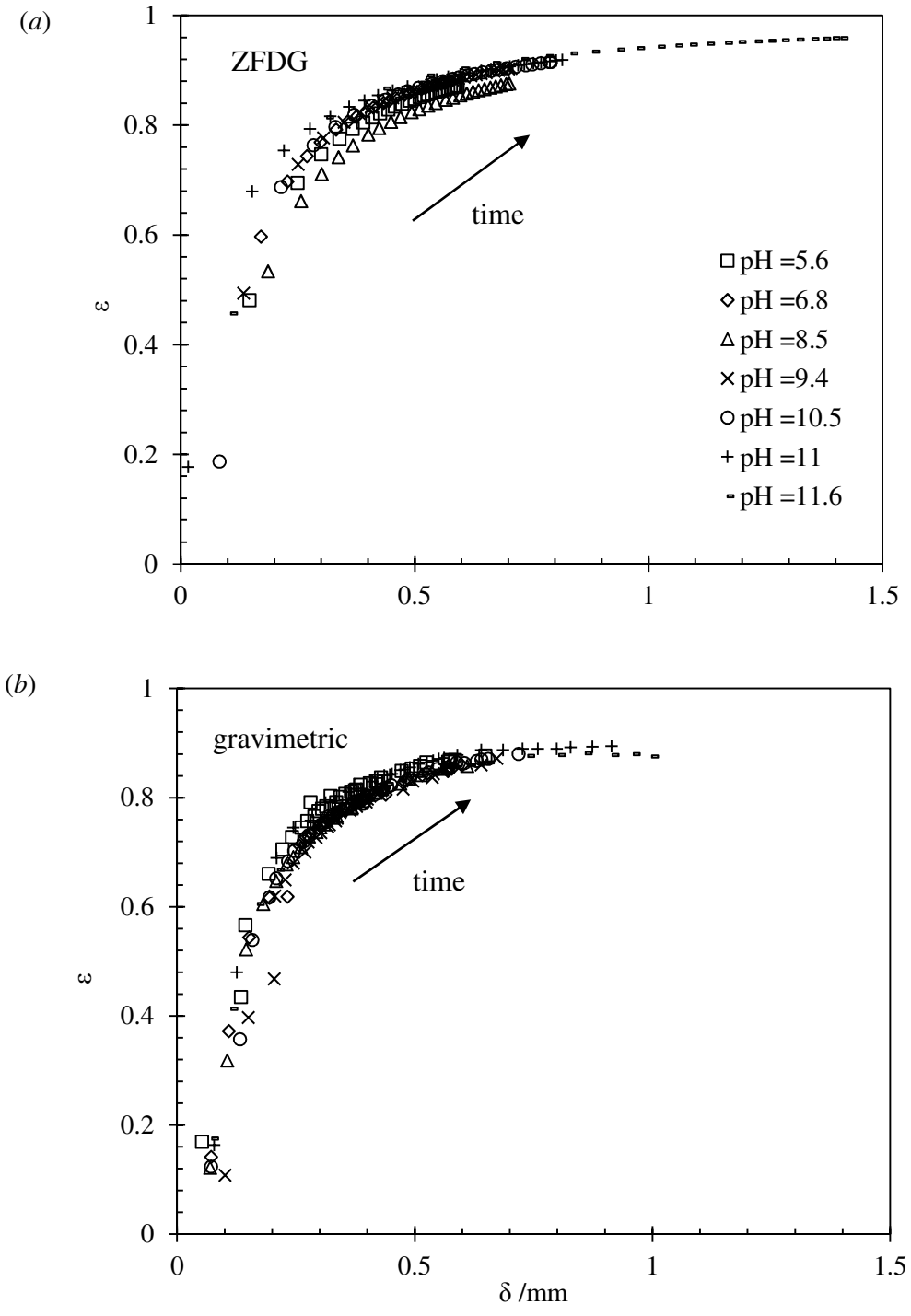

Figure 12. Evolution of liquid volume fraction against layer thickness for (*a*) ZFDG and (*b*) gravimetric measurements. Legend in (*a*) indicates pH.

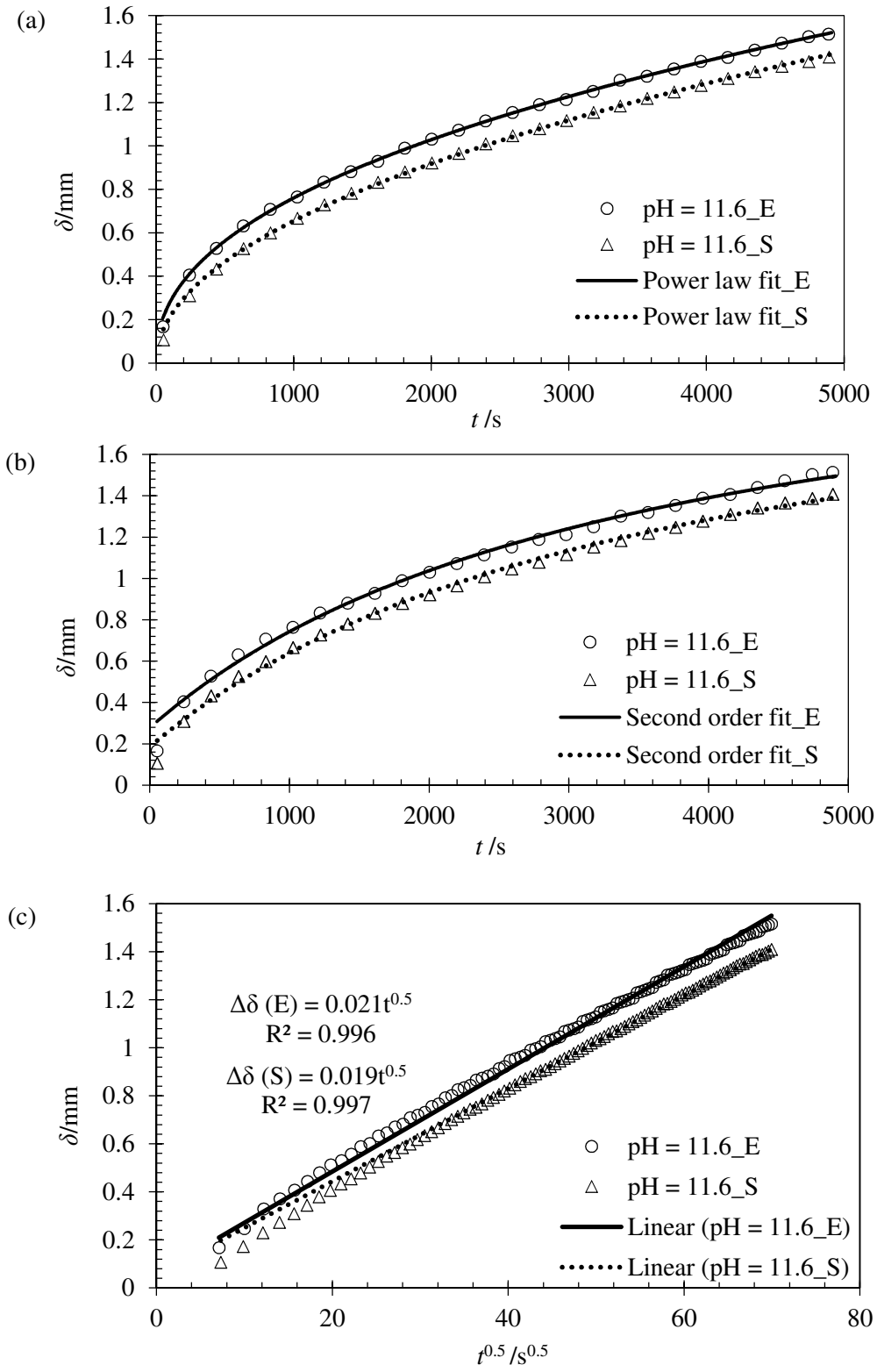

Figure 13. Comparison of swelling models with ZFDG experimental data for gelatine layers at pH 11.6, 16.5 °C. (*a*) power law, equation (9); (*b*) Model II, equation (13); (c) swelling front, equation (20). Data decimated for clarity. Symbols: ejection – circle, solid line; suction – triangle, dashed line. Initial dry thickness 58 ±10 μm, $\dot{m}$= 0.33 g/s.

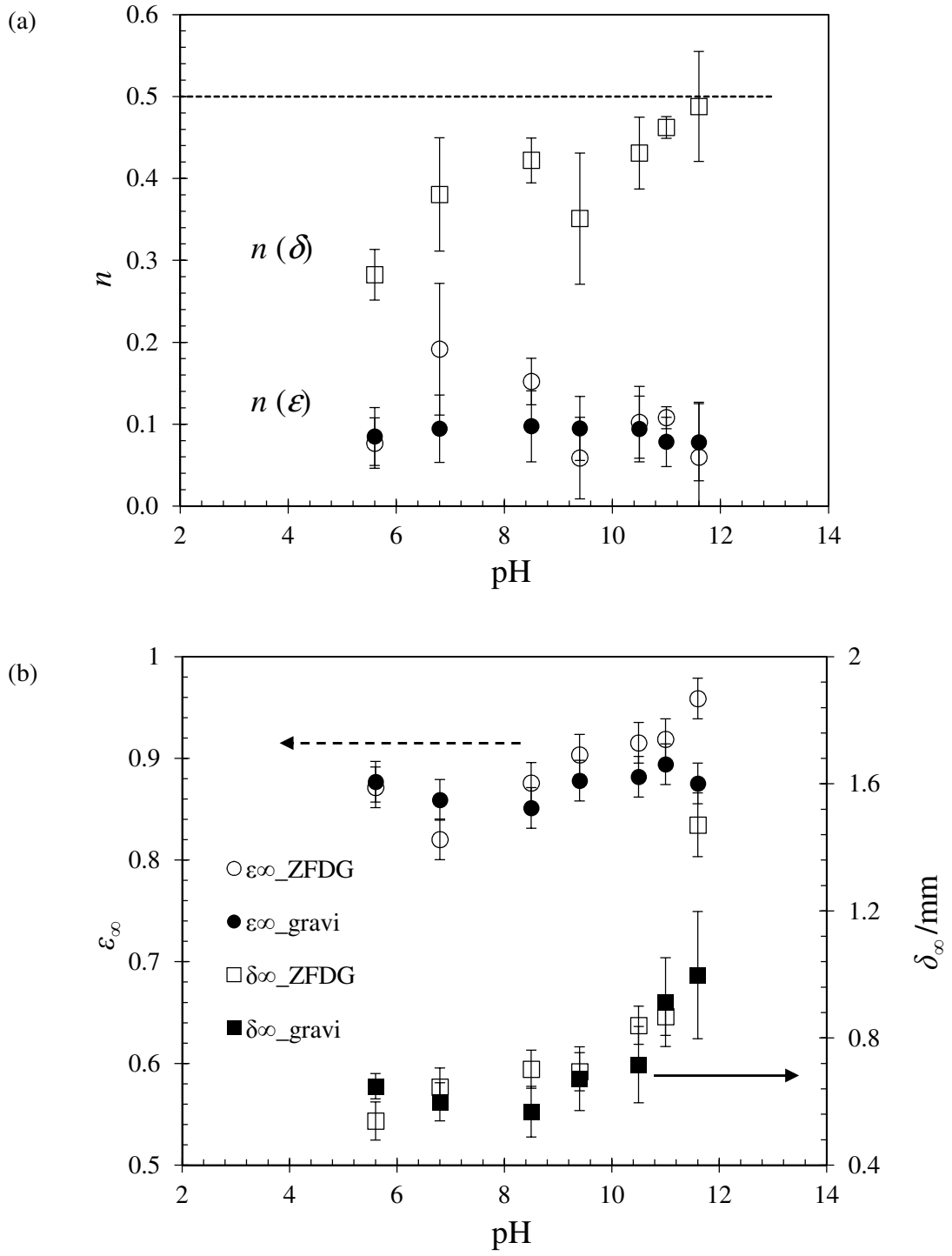

Figure 14. (*a*) Diffusion index, *n*, obtained from power law fitting, equation (9), at different pH for both ZFDG and gravimetric measurements. Symbols: hollow – ZFDG, solid – gravimetric; circle – ε, and square – δ; $n = 0.5$ indicates Fickian diffusion. (*b*) Estimated final volume fraction of solvent, ε_∞ and thickness, δ_∞.